East European Journal of Physics. 3. 355-362 (2023)
DOI:10.26565/2312-4334-2023-3-37 ISSN 2312-4334

EFFECT OF CALCINATION TEMPERATURE ON STRUCTURAL AND OPTICAL PROPERTIES OF NICKEL ALUMINATE NANOPARTICLES[†]

Katrapally Vijaya Kumar[a,*], Sara Durga Bhavani[b]
[a]*Department of Physics, JNTUH University College of Engineering Rajanna Sircilla, Agraharam, Rajanna Sircilla-District, 505302, TS, India*
[b]*Department of Chemistry, Government Degree College, Rajendra Nagar, Hyderabad, 500001, TS, India.*
**Corresponding Aythor e-mail: kvkumar@jntuh.ac.in, kvkphd@gmail.com*
Received May 19, 2023; revised June 30, 2023; accepted June 30, 2023

Nickel aluminate ($NiAl_2O_4$) nanoparticles were synthesized using sol-gel method with auto-combustion. The prepared nanoparticles were made into four parts and calcinated at 700, 900, 1100 and 1300°C and taken up for the present study. The taken-up nanoparticles were characterized using powder X-Ray Diffraction (XRD), Scanning Electron Microscopy (SEM), Energy Dispersion X-Ray Spectroscopy (EDS), Fourier Transform and Infrared (FT-IR) spectroscopy and UV-Vis spectroscopy techniques. The X-ray diffraction patterns confirmed the spinel structure and Fd3m space group. Scherrer formula was used to calculate the crystallite size and found in the range 5.78 to 20.55 nm whereas the lattice parameter was found in the range of 8.039 to 8.342 Å. The average grain size was found in the range 142.80 to 187.37 nm whereas interplanar spacing was found in the range of 2.100 to 2.479 Å. The FTIR spectroscopy showed six absorption bands in the range 400 to 3450 cm^{-1} and confirmed the spinel structure. The optical band gap (E_g) was decreased with calcination temperature and found in the range 4.2129-4.3115eV.
Keywords: *Nickel Aluminate nanoparticles; Sol-Gel Auto-Combustion method; Calcination Temperature; Crystallite size; Grain size; Elemental analysis; IR and UV-Vis spectroscopy*
PACS: 75.50.Gg, 61.05.cp, 68.37.Hk, 78.40.Fy, 33.20.Ea, 42.70.Qs

INTRODUCTION

Since few years, the usage of composite materials has significantly increased in various applications due to their exceptional properties when compared with metals, ceramics and polymers. The composite materials containing spinel phase are stable at high temperatures, chemically resistant, abrasion resistant and exhibit high hardness [1-3]. The composite oxides such as mixed spinels have been attracted the scientists due to their significance behaviour in magnetic properties [4], catalytic properties [5], luminescent properties [6], sensing properties [7], lithium batteries [8] etc. The composite oxides having chemical formula AB_2O_4, where A, represents divalent metal ion residing tetrahedral sites and B, represents trivalent metal ion residing octahedral sites [9, 10]. In the recent days, spinel oxides having chemical formula MCr_2O_4, where M represents a divalent metal ion such as Ni, Cu, Zn, Co, Mg, Fe have attracted several researchers because of their upgraded properties [11]. These materials at the nanoscale range are gained importance because of their small size and large surface area with their upgraded properties compared to their counter bulk materials. Especially, $ZnCr_2O_4$ mixed spinels have become important functional materials due to their humidity sensing properties [12], optical and photocatalytic properties [13], electrical and magnetic properties [13-14]. The properties of these materials would depend on the synthesis process and reaction conditions. Many synthesis processes were found in the literature to synthesize $ZnCr_2O_4$ nanoparticles such as ball milling method [15], solid-state reaction method [16], micro emulsion method [17], precipitation method [18], auto-combustion method [19] etc. Few of the synthesis processes give the product material of low quality with existence of impurities, require high temperature and consume more energy, require involvement of organic solvents which makes the process costly. Kumar et al [20] investigated structural properties of $ZnCr_2O_4$ nanoparticles prepared by sol-gel method with auto combustion as it gives the product material of high purity, good homogeneity at low processing temperature. Expecting an interesting study on calcination temperature dependent physical and optical properties, the nickel aluminate ($NiAl_2O_4$) spinel nanoparticles were considered for investigation and prepared by using sol-gel method with auto combustion.

EXPERIMENTAL

Nickel aluminate ($NiAl_2O_4$) spinel nanoparticles were prepared by sol-gel method with auto-combustion [21] following the procedure shown in flowchart (Fig. 1). The materials such as nickel nitrate ($Ni(NO_3)_2{\cdot}6H_2O$) and aluminium nitrate ($Al(NO_3)_2{\cdot}6H_2O$) were used as starting materials. The citric acid and ammonia of analytical grade (AR) were also used in the required quantity in the synthesis process. A solution was prepared using the raw materials in their stoichiometry by dissolving in a deionized water. The molar ratio of citric acid and the total moles of nitrate ions was adjusted to 1:3 and added to the arranged solution to chelate Ni^{2+}, Al^{3+} and Fe^{3+} ions in the solution. The prepared solution was made neutralized by maintaining the pH value 7 by the addition of ammonia (NH_3) to the solution in required proportion. The final neutralized solution was then heated at about 100°C on a hot plate with constant stirring till the

[†] ***Cite as:*** K.V. Kumar, S.D. Bhavani, East Eur. J. Phys. 3, 355 (2023), https://doi.org/10.26565/2312-4334-2023-3-37

viscous state was reached which led to form a viscous gel. There onwards, the temperature was increased to ~ 200°C to burn the gel entirely in a self-propagating combustion manner to turn into a loose powder [22, 23]. The prepared powder was divided into four parts and calcinated at 700, 900, 1100 & 1300°C for 8 h.

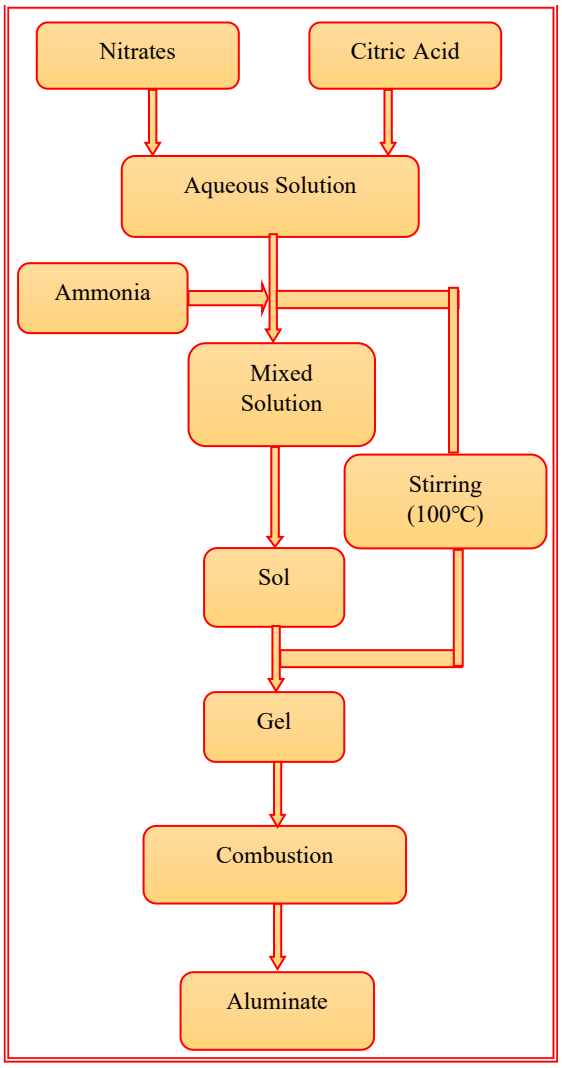

Figure 1. Flowchart of the sol-gel auto combustion method

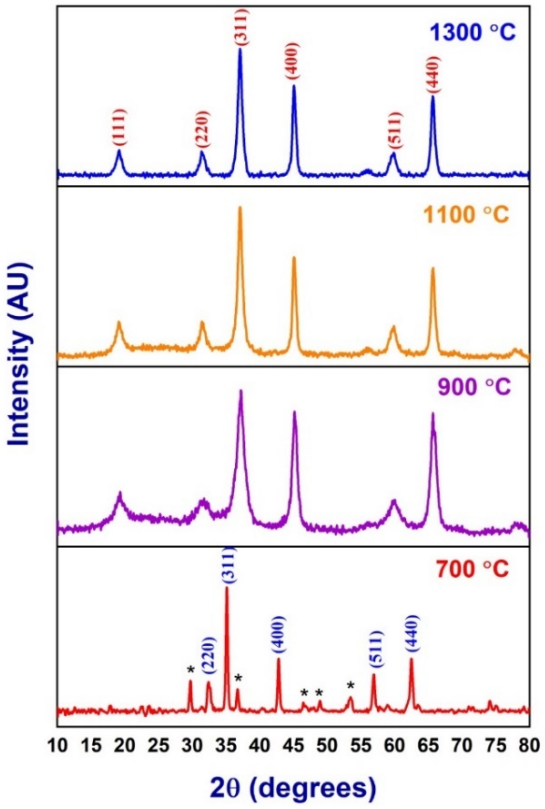

Figure 2. XRD patterns of $NiAl_2O_4$ nanoparticles calcinated at 700, 900, 1100 & 1300°C

Using Phillips Expert Diffractometer, the X-Ray diffraction (XRD) measurements were carried out at room temperature in the range of 20˚-80˚ whereas ZEISS EVO 18, Special Edition was used to bring out the micro structural studies and elemental analysis of the prepared samples. Using Shimadzu FTIR spectrometer (Model: FTIR-8400 S), Fourier transform infrared spectroscopic studies were carried out within a range of 300-4000 cm^{-1}. Using, SYSTRONICS DOUBLE BEAM UV-VIS Spectrophotometer: 2202, UV-Vis spectra studies were recorded in the range 200-800 nm.

RESULTS AND DISCUSSION

XRD Analysis

XRD plots of the nickel aluminate ($NiAl_2O_4$) spinel nanoparticles calcinated at 900, 1100 and 1300°C are shown in Fig. 2. They clearly exhibited the prominent peaks for the crystal planes of Miller indices (1 1 1), (2 2 0), (3 1 1), (4 0 0), (5 1 1), (4 4 0) and they confirmed the establishment of single-phase spinel structure with space group of Fd3m [24]. But, in the XRD pattern of the sample calcinated at 700°C the crystal planes of Miller indices (1 1 1) were missed. Few extra peaks were observed in all the XRD plots and they were marked with star symbol. Hence, it was clearly understood that the crystal phase was formed perfectly in all the samples [25-27] except in the sample calcinated at 700°C. Using Scherrer formula [28] shown in equation (1), the crystallite size was calculated for all the prominent peaks and the same furnished in the Table 1 along with Miller indices, FWHM, 2θ and d-spacing values.

$$t = \frac{0.89\,\lambda}{\beta\,Cos\,\theta} \tag{1}$$

Table 1. (hkl), 2θ, FWHM, crystallite size, Interplanar spacing of $NiAl_2O_4$ nanoparticles calcinated at 700, 900, 1100 & 1300°C

Calcination Temperature (°C)	Average FWHM (Radians)	Average Crystallite Size (nm)	Lattice Parameter (Å)	Unit Cell Volume (Å^3)	Average Interplanar spacing (Å)	Average Grain Size (nm)
700	0.45	20.55	8.342	580.64	2.100	142.80
900	1.80	5.78	8.039	519.54	2.472	145.29
1100	1.05	9.21	8.042	520.34	2.479	159.75
1300	0.90	10.38	8.058	523.17	2.479	187.37

Where, t is known as crystallite size, λ is known as X-ray wavelength (1.54 Å), θ is angle of diffraction and β is known as full width at half maximum (FWHM). The average crystallite size of all the samples was found in the range 5.78 nm-20.55 nm and the same furnished in the Table 2.

Table 2. Interplanar spacing, average grain size, reciprocal lattice of $NiAl_2O_4$ nanoparticles calcinated at 700, 900, 1100 & 1300°C

Calcination Temperature (°C)	(h k l)	2θ (Degrees)	FWHM (Radians)	Crystallite Size (nm)	d (spacing) (Å)
700	220	32.40	0.62	13.34	2.76
	311	**35.12**	**0.32**	**26.04**	**2.558**
	400	42.8	0.35	24.82	2.113
	511	56.9	0.46	19.65	1.617
	440	62.48	0.48	19.36	1.486
900	111	19.3	2.29	3.52	4.608
	220	31.76	2.9	2.85	2.416
	311	**37.20**	**1.3**	**6.45**	**2.416**
	400	45.14	0.95	9.05	2.006
	511	59.96	2.3	3.99	1.543
	440	65.68	1.07	8.84	1.420
1100	111	19.12	1.42	5.67	4.628
	220	31.38	1.26	6.55	2.837
	311	**37.08**	**0.82**	**10.22**	**2.423**
	400	45.12	0.66	13.03	2.009
	511	59.80	1.46	6.28	1.558
	440	65.70	0.70	13.51	1.421
1300	111	19.16	1.06	7.60	4.632
	220	31.38	1.00	8.25	2.840
	311	**37.08**	**0.76**	**11.02**	**2.425**
	400	45.06	0.60	14.33	2.010
	511	59.84	1.32	6.94	1.547
	440	65.66	0.67	14.11	1.421

Though, the phase is not formed completely for the sample calcinated at 700°C, the crystallite size was observed highest, i.e., 20.55 nm where as for the sample calcinated at 900°C, the crystal phase was formed perfectly and the crystallite size was observed lowest, i.e., 5.78 nm. Further, the crystallite size was found increased for the samples calcinated from 900 to 1300°C [29]. The calculated lattice parameter values were found in the range of 8.039 to 8.342 Å. In the similar lines to the crystallite size, the lattice parameter was found highest, i.e., 8.342 Å for the sample calcinated at 700°C where as it is found lowest, i.e., 8.039 Å, for the sample calcinated at 900°C. Further, the lattice parameter was increased with the calcinated from 900 to1300°C.

The bond lengths between cations and oxygen located at A and B sites were measured along with ionic radii of cations furnished in Table 3. The bond lengths of A site-oxygen and B site-oxygen were found maximum in case of the sample calcinated at 700°C where as they were found minimum for the sample calcinated at 900°C.

Table 3. Bond lengths and ionic radii in $NiAl_2O_4$ nanoparticles calcinated at 700, 900, 1100 & 1300°C

Calcination Temperature (°C)	Bond length of A site-O (^{0}A)	Bond length of B site-O (^{0}A)	Ionic radius(r_A) (^{0}A)	Ionic radius(r_B) (^{0}A)
700	1.898	1.984	0.4796	0.4855
900	1.829	1.913	0.4076	0.4132
1100	1.830	1.914	0.4084	0.4141
1300	1.834	1.918	0.4120	0.4177

Further they were found increased with the calcination temperature. In the similar lines, the ionic radii at A and B sites were found maximum in case of the sample calcinated at 700°C where as they were found minimum for the sample calcinated at 900°C. Further they were found increased with the calcination temperature. Hence, it can be concluded that the effect of calcination temperature on all the calculated parameters from the XRD data was clearly observed.

SEM Analysis

The SEM micrographs of the nickel aluminate ($NiAl_2O_4$) spinel nanoparticles calcinated at 900, 1100 and 1300°C are shown in Fig. 3. It is clearly observed that the size and shape of the grains were appeared as non-uniform flakes [30] with several pores and voids. The calculated average grain size was found in the range 142.80 to 187.82 nm and the same furnished in the Table 2. The grain size was found minimum for the sample calcinated at 700°C and it was found gradually increased with the calcination temperature [31].

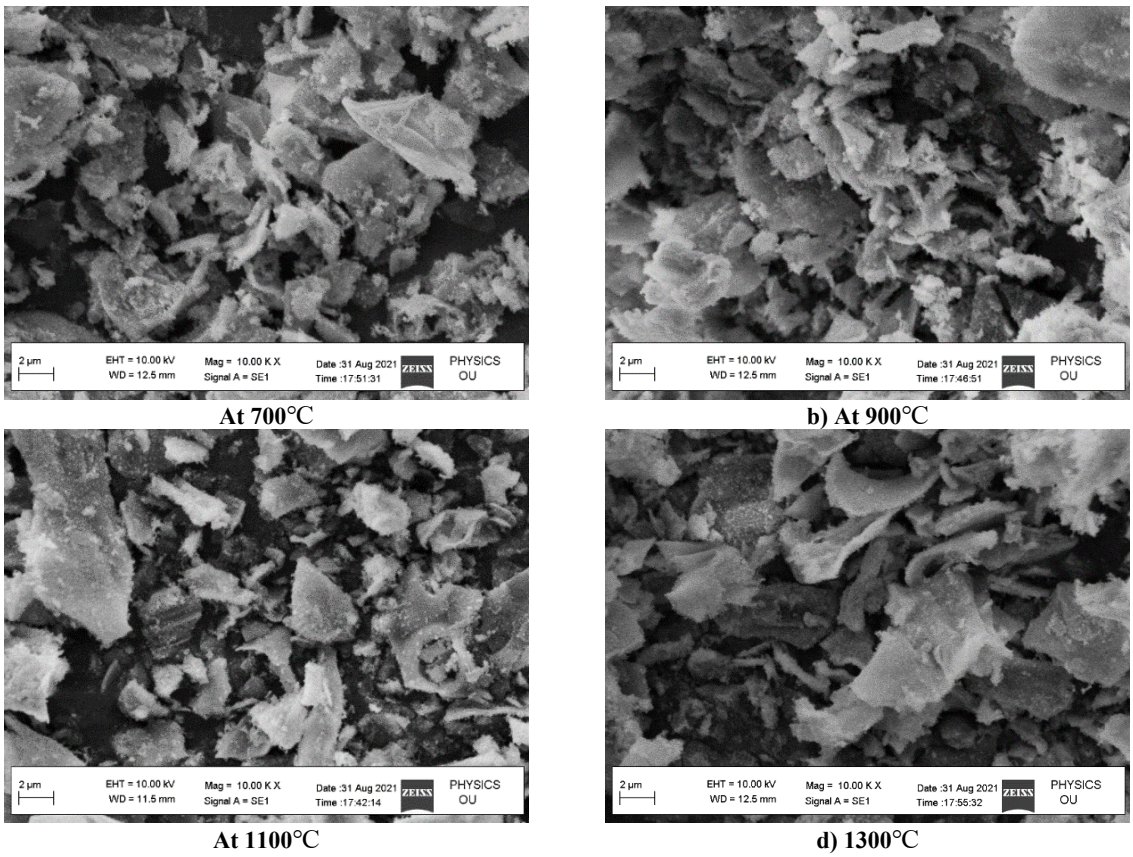

Figure 3. SEM images of $NiAl_2O_4$ nanoparticles calcinated at 700, 900, 1100 & 1300°C

EDS Analysis

The Energy Dispersive X-ray Spectra of all the nickel aluminate ($NiAl_2O_4$) spinel nanoparticles are shown in Fig. 4. It was clearly observed that the presence of Ni, Al and O without any impurities and the atomic percentages are furnished in Table 4.

Table 4. Elemental percentage of $NiAl_2O_4$ nanoparticles calcinated at 700, 900, 1100 & 1300°C

Calcination Temperature (°C)	Element	Atomic %
700	Ni	4.93
	Al	8.05
	O	25.44
	C	61.58
900	Ni	14.23
	Al	28.40
	O	57.36
1100	Ni	14.78
	Al	25.78
	O	59.43
1300	Ni	14.37
	Al	28.30
	O	57.34

It was clearly noticed that the theoretical and experiential atomic percentages of nickel, aluminium and oxygen are in close agreement in case of all the taken-up samples [32]. It was clearly observed that no impurities were traced in all the samples except in the sample calcinated at 700°C as an impurity of carbon was found in a considerable quantity. Further, it was also clearly noticed that there was no loss of any fundamental elements during the synthesis process.

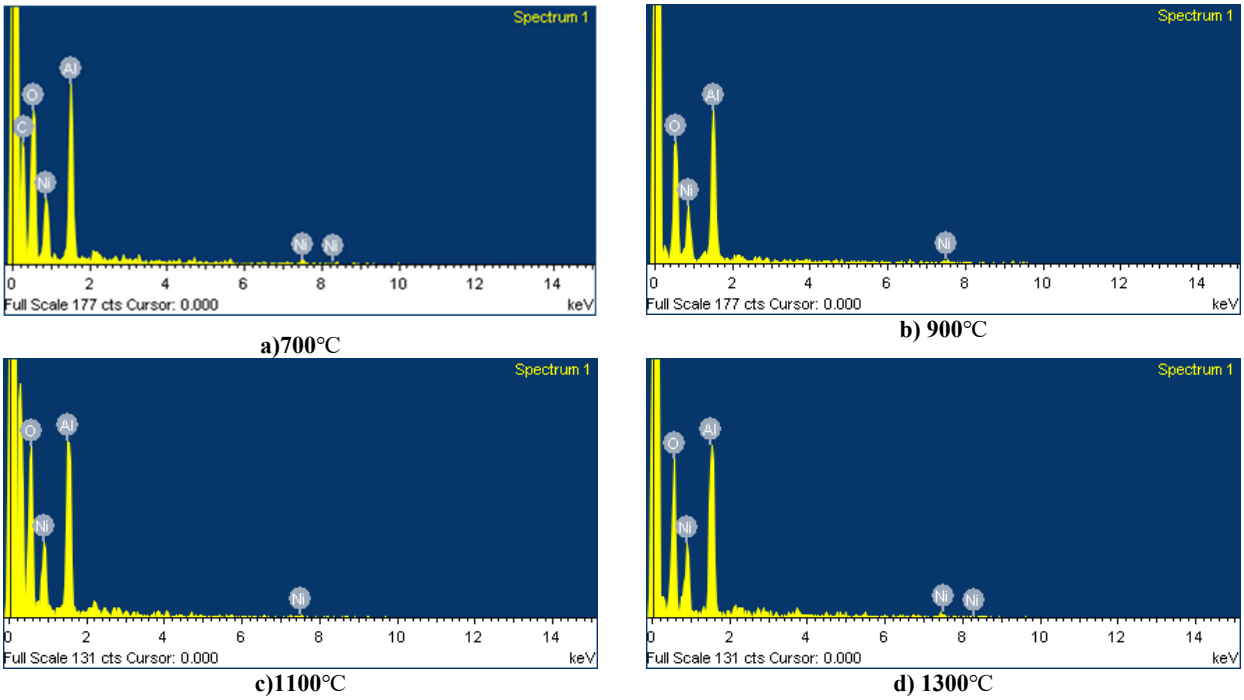

Figure 4. EDS spectra of $NiAl_2O_4$ nanoparticles calcinated at 700, 900, 1100 & 1300°C

FTIR Spectroscopy

Fourier transform infrared (FTIR) spectra of all the nickel aluminate ($NiAl_2O_4$) spinel nanoparticles are presented in Fig. 5.

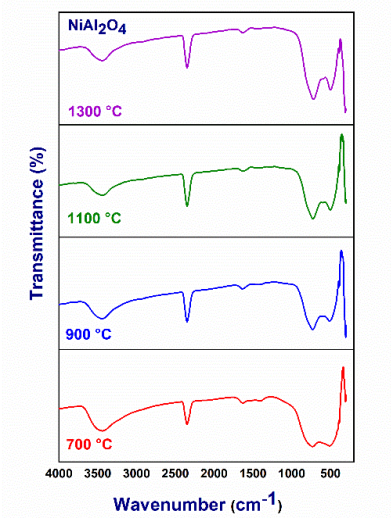

Figure 5: FTIR patterns of $NiAl_2O_4$ nanoparticles calcinated at 700, 900, 1100 & 1300°C

The FTIR spectra showed a categorization of absorption peaks in the range of 300-4000 cm^{-1} and the concerned frequencies are furnished in Table 5. Based on the absorption peaks, the functional groups that are existing were appraised for all the samples. The characteristic frequencies in the range 499-730 cm^{-1} may be attributed to characteristic metal-oxygen vibrations indicating the establishment of single phase $NiAl_2O_4$ [33]. The peaks observed in the frequency range 499-730 cm^{-1} can be assigned to Ni-O, Al-O, and Ni-O-Al bonds. The peaks observed in the frequency range of 499.5-511.1 cm^{-1} can be attributed to Al-O stretching vibrations whereas the peaks observed in the frequency range 719.4-729.1 cm^{-1} can be attributed to Ni-O stretching vibrations. The peaks observed in the frequency range 1400-1413 cm^{-1} represent the stretching vibrations in CH2 and CH3 [34]. The peaks observed in the frequency range 1630-1632 cm^{-1} can be assigned to the deformative vibration of water molecules which would be most possibly due to water absorption during the pressing of the powder samples with KBr. The strong peak observed at the frequency 2349 cm^{-1} originates from the mode of CO_2^{3-} ion. The presence of this CO_2 would be either because of the presence of aerial CO_2 or may be due to the presence of CO_2 inside the grains of powders [35]. The peaks observed in the frequency range 3441-3143 cm^{-1} denoted for the -OH stretching vibration of free hydrogen bonded hydroxyl groups [32]. For the nanosized grains, the atomic orientations along the boundaries very much differed from those of bulk crystals with regard to coordination number and bond lengths and showed some extent of disorder [36, 37]. And it can be concluded that impurity phase was not detected in FTIR spectra which agrees with the results attained by XRD.

Table 5. The Characteristic wavenumbers of $NiAl_2O_4$ nanoparticles calcinated at 700, 900, 1100 & 1300°C

Calcination Temperature (°C)	ν_1 (cm^{-1})	ν_2 (cm^{-1})	ν_3 (cm^{-1})	ν_4 (cm^{-1})	ν_5 (cm^{-1})	ν_6 (cm^{-1})
700	511.1	729.1	1413	1630	2349	3441
900	509.2	729.1	1400	1632	2349	3443
1100	501.5	725.3	-	1632	2349	3443
1300	499.5	719.4	-	1630	2349	3441

UV-Visible Spectroscopy

Optical absorption properties of all the nickel aluminate ($NiAl_2O_4$) spinel nanoparticles were studied in the wavelength region 200-800 nm at room temperature using UV-Visible spectroscope. Fig. 6 shows the UV-Visible absorbance spectra of all the samples and observed two prominent absorption peaks in the wavelength range 230-360 nm and few peaks thereafter.

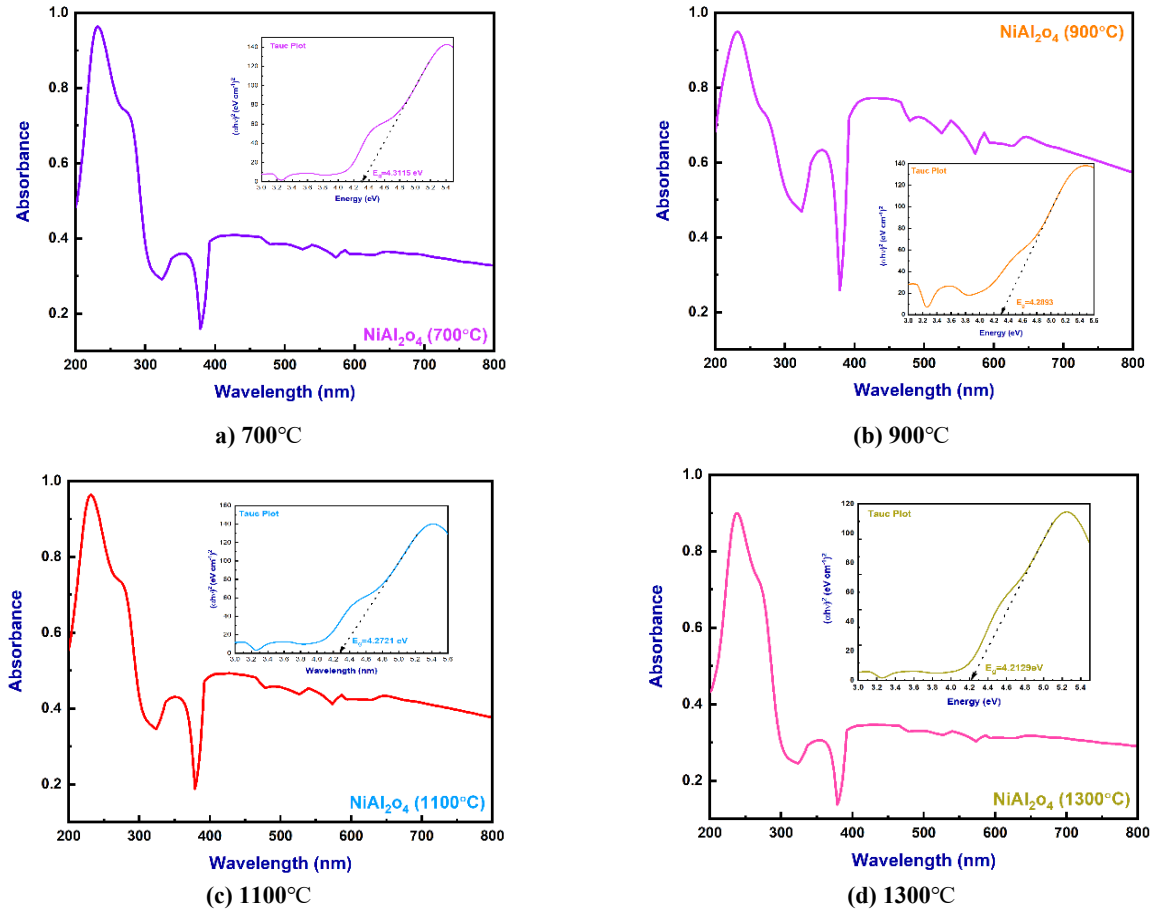

Figure 6. UV-Vis patterns of $NiAl_2O_4$ nanoparticles calcinated at 700, 900, 1100 & 1300°C

The first peak can be assigned to the $O^{2-} \rightarrow Ni^{2+}$ charge transfer process while the second peak to the $O^{2-} \rightarrow Ni^{3+}$ charge transfer [38]. The energy-level diagram for Ni^{2+} (3d7 configurations) in both octahedral and tetrahedral sites presents few spin-allowed transitions. Regarding Ni^{2+} in a tetrahedral site, it was detected a peak recognized to the [$^4A_2$ (F) → $^4T_1$ (P)] transition at around ~ 426 nm (red region), 538 nm (green region), ~ 586 nm (yellow-orange region) and ~646 nm which gives rise to the red coloration. These peaks can be accredited to a Jahn-Teller distortion of the tetrahedral structure [39, 40]. From the literature [41], the absorption peak at 540-650 nm can be attributed to the spin electronic transition $^3T_1(F) \rightarrow {}^3T_1(p)$ assigned to tetrahedrally coordinated Ni^{2+}, the peak at 630-800 nm was due to spin transition $^3A_{2g}(F) \rightarrow {}^3T_{1g}(F)$ assigned to octahedrally coordinated Ni^{2+} and the peaks at 230-360 nm and 360-540 nm can be assigned to the charge transfer.

The band gap can be determined by extrapolation to the energy axis of the linear plots of $(\alpha h\nu)^n$ as a function of the photon energy ($h\nu$) as shown in Fig. 6 (Tauc plot). To determine the type of transition, we have used equation (2) which is known as Tauc formula [42]:

$$(\alpha h\nu)^{1/n} = A\,(h\nu - E_g). \qquad (2)$$

Where, α is known as absorption coefficient, A is known as proportional constant, E_g is known as optical band gap of the material and exponent, n represents the nature of electronic transition (2 for a direct transition and 1/2 for an indirect transition). The optical band gap (E_g) value for all the samples is calculated, found in the range 4.2129-4.3115eV and furnished in Table 6.

Table 6. The band gap values of $NiAl_2O_4$ nanoparticles calcinated at 700, 900, 1100 & 1300°C

Calcination Temperature (°C)	Band gap (E_g) (eV)
700	**4.3115**
900	**4.2893**
1100	**4.2721**
1300	**4.2129**

It can be observed that the optical band gap was found minimum (E_g= 4.2129 eV) for the sample calcinated at 700°C, further it was increased with calcination temperature and found maximum (E_g= 4.3115 eV) for the sample calcinated at 1300°C. In the case of Rahman et al, the optical energy gap for the undoped ZnO and zinc aluminate spinel nanoparticles were found 2.82 and 2.84 eV respectively [43] and they found that it is increased to 3.07 eV with aluminium concentration. Suresh et al. found, the higher optical energy gap of 4.11 eV in case of zinc aluminate [44]. The increase in band gap is due to formation of $ZnAl_2O_4$ spinel phase in $ZnO–Al_2O_3$ system and can be explained on the basis of the Burstein-Moss effect [45]. The optical band gap of nickel aluminate spinel nanoparticles in the present work was observed in the range 4.6270-4.7330 eV. It can be understood that the Fermi level would move close to the conduction band when the carrier concentration was increased, therefore the lower energy transitions were blocked and the optical band gap would be increased. This was also found in good agreement to the quantum confinement effect of the nanoparticles [46].

CONCLUSIONS

1. The prepared nickel aluminate ($NiAl_2O_4$) nanoparticles were divided into four parts and calcinated at 700, 900, 1100 and 1300°C.
2. The X-Ray diffraction patterns authorize the establishment of single-phase cubic spinel structure with space group Fd3m for all the samples except the sample calcinated at 700°C.
3. The average crystallite size and lattice parameter were found maximum in case of the sample calcinated at 700^0C. Both the parameters were found to be increased with the calcination temperature from 900 to 1300°C.
4. The average grain size was found increased with calcination temperature and it was found in the range of 142.80-187.82 nm.
5. The average grain size was found in the range 142.80-187.37 nm whereas interplanar spacing was found in the range of 2.100-2.479 Å. Both the parameters were found to be increased with calcination temperature.
6. The two absorption peaks related to octahedral and tetrahedral sites, in the range 499.5-511.1 and 719.4-729.1 cm^{-1} which confirmed the spinel cubic crystal structure and in good agreement with XRD results.
7. The value of optical band gap (E_g) was found in the range 4.2129-4.3115eV, and the band gap was increased with the calcinated temperature.

Acknowledgements

The authors expressed their thankfulness to the Principal, JNTUH University College of Engineering Rajanna Sircilla and the Principal, Government Degree College Rajendranagar, for their constant encouragement and support in carrying out this research work.

ORCID

Katrapally Vijaya Kumar, https://orcid.org/0000-0001-6160-8632
Sara Durga Bhavani, https://orcid.org/0000-0001-9854-0061

REFERENCES

[1] Z. Yin, C. Huang, B. Zou, H. Liu, H. Zhu, and J. Wang, Ceramic International, **40**(2), 2809 (2014). https://doi.org/10.1016/j.ceramint.2013.10.033
[2] J.B. Wachtman, *Mechanical Properties of Ceramics*, (Wiley, New York, 1996)
[3] K. Konopka, M. Maj, and K.J. Kurzydłowski, Mater. Charact. **51**, 335 (2003). https://doi.org/10.1016/j.matchar.2004.02.002
[4] C.C. Huang, C.C. Mo, T.H. Hsiao, G.M. Chen, S.H. Lu, Y.H. Tai, H.H. Hsu, *et al*., Results in Materials, **8**, 100150 (2020). https://doi.org/10.1016/j.rinma.2020.100150
[5] D.C. Kim, and S.K. Ihm, Env. Sci. Tech. **35**(1), 222 (2001). https://doi.org/10.1021/es001098k
[6] C. Chaves, S.J.G. Lima, R.C.M.U. Araujo, M.A. Maurera, E. Longo, P.S. Pizani, L.G.P. Simões, *et al*., J. Solid-State Chem. **179**, 985 (2006). https://doi.org/10.1016/j.jssc.2005.12.018
[7] K. Ahn, B.W. Wessels, and S. Sampath, Sensor Actuators B, **107**(1), 342 (2005). https://doi.org/10.1016/j.snb.2004.10.020
[8] P. Lavela, J.L. Tirado, and C.V. Abarca, Electrochimica Acta, **52**(28), 7986 (2007). https://doi.org/10.1016/j.electacta.2007.06.066
[9] Y. Fan, X. Lu, H. Zhang, L. Zhao, J. Chen, and C. Sun, Environ. Sci. Technol. **44**(8), 3079 (2010). https://doi.org/10.1021/es9031437
[10] S. Chen, Y. Wu, P. Cui, W. Chu, X. Chen, and Z. Wu, J. Phys. Chem. C, **117**(47), 25019 (2013). https://doi.org/10.1021/jp404984y
[11] J. Ma, B. Zhao, H. Xiang, F.Z. Dai, Y. Liu, R. Zhang, and Y. Zhou, J. Adv. Cer. **11**, 754 (2022). https://doi.org/10.1007/s40145-022-0569-3
[12] S. Pokhrel, B. Jeyaraj, and K.S. Nagaraja, Mater. Lettrs. **57**(22-23), 3543 (2003). https://doi.org/10.1016/S0167-577X(03)00122-8
[13] C. Peng, and L. Gao, J. Amer. Cer. Soc. **91**(7), 2388 (2008). https://doi.org/10.1111/j.1551-2916.2008.02417.x
[14] R.J. Harrison, and A. Putnis, Surv. in Geophys. **19**, 461 (1998). https://doi.org/10.1023/A:1006535023784
[15] Z.V. Marinkovic, L. Mancic, P. Vulic, and O. Milosevic, J. Euro. Cer. Soc. **25**, 2081 (2005). https://doi.org/10.1016/j.jeurceramsoc.2005.03.085
[16] Yunasfi, A. Mulyawan, Mashadi, D.S. Winatapura, and A.A. Wisnu, Applied Phys. A, **127**, 763 (2021). https://doi.org/10.1007/s00339-021-04907-w
[17] X. Niu, W. Du, and W. Du, Sensor Actuators B, **99**, 405 (2004). https://doi.org/10.1016/j.snb.2003.12.007
[18] C. Jagadeeshwaran, and R. Murugaraj, J. Supercondu. and Novel Magn. **33**, 1765 (2020). https://doi.org/10.1007/s10948-020-05427-z

[19] K.R. Krishna, K.V. Kumar, and D. Ravinder, Adv. in Mater. Phys. and Chem. **2**(3), 185 (2012). http://dx.doi.org/10.4236/ampc.2012.23028
[20] K.V. Kumar, and C.H.S. Chakra, Asian J. of Phys. and Chem. Sci. **2**(2), 1 (2017). https://doi.org/10.9734/AJOPACS/2017/34683
[21] K. Vijaya Kumar, R. Sridhar, D. Ravinder, Int. J. of Nanopart. Res., **2**(6), 1 (2018). https://escipub.com/Articles/IJONR/IJNR-2018-01-0302
[22] L.J. Berchmans, R.K. Selvan, and C.O. Augustin, Mater. Lettrs. **58**(12), 1928 (2004). https://doi.org/10.1016/j.matlet.2003.12.008
[23] Z. Yue, J. Zhou, L. Li, X. Wang, and Z. Gui, Mater. Sci. and Eng. B, **86**(1)**,** 64 (2001). https://doi.org/10.1016/S0921-5107(01)00660-2
[24] N.M. Deraz, Int. J. Electrochem. Sci. **8**, 5203 (2013). http://electrochemsci.org/papers/vol8/80405203.pdf
[25] A. Yamakawa, M. Hashiba, and Y. Nurishi, J. Mater. Sci. **24**, 1491 (1989). https://doi.org/10.1007/BF02397091
[26] N.M. Deraz, Ceramic International, **38**, 511 (2012). https://doi.org/10.1016/j.ceramint.2011.07.036
[27] N.M. Deraz, Int. J. Electrochem. Sci. **7**, 4596 (2012). http://www.electrochemsci.org/papers/vol7/7054596.pdf
[28] A. Becheri, M. Durr, P. Lo Nostro, and P. Baglioni, J. Nanopart. Res. **10**, 679 (2008). https://doi.org/10.1007/s11051-007-9318-3
[29] J. Jacob, and M.A. Khadar, J. Appl. Phys. **107**(11), 114310 (2010). https://doi.org/10.1063/1.3429202
[30] Y.B. Kannan, R. Saravanan, N. Srinivasan, and I. Ismail, J. Magn. and Magn. Mat. **423**, 217 (2017). https://doi.org/10.1016/j.jmmm.2016.09.038
[31] D. Venkatesh, K.V. Ramesh, and C.V.S.S. Sastry, AIP Conference Proceedings, **1859**, 020035 (2017). https://doi.org/10.1063/1.4990188
[32] F. Meyer, R. Hempelmann, S. Mathurband, and M. Veith, J. Mater. Chem. **9**, 1755 (1999). https://doi.org/10.1039/A900014C
[33] Giedrė Nenartavičienė, Darius Jasaitis, and Aivaras Kareiva, Acta Chim. Slov. **51**, 661 (2004). https://acta-arhiv.chem-soc.si/51/51-4-661.pdf
[34] M. Chroma, J. Pinkas, I. Pakutinskiene, A. Beganskiene, and A. Kareiva, Ceramic International, **31**(8), 1123 (2005). https://doi.org/10.1016/j.ceramint.2004.11.012
[35] J.J. Vijaya, L.J. Kennedy, G. Sekaran, and K.S. Nagaraja, Materials Research Bulletin, **43**, 473 (2008). https://doi.org/10.1016/j.materresbull.2007.02.030
[36] S. Angappan, L.J. Bechermans, and C.O. Augustin, Mater. Lett. **58**, 2283 (2004). https://doi.org/10.1016/j.matlet.2004.01.033
[37] Z. Chen, E. Shi, W. Li, Y. Zheng, N. Wu, and W. Zhong, J. Am. Ceram. Soc. **85**, 2949 (2002). https://doi.org/10.1111/j.1151-2916.2002.tb00561.x
[38] M. Llusar, A. Forés, J.A. Badenes, J. Calbo, M.A. Tena, and G. Monrós, J. Eur. Ceram. Soc. **21**(8), 1121 (2001). https://doi.org/10.1016/S0955-2219(00)00295-8
[39] A.A. Verberckmoes, B.M. Weckhuysen, and R.A. Schoonheydt, Micropor. Mesopor. Mater. **22**(1-3), 165 (1998). https://doi.org/10.1016/S1387-1811(98)00091-2
[40] F. Matteucci, G. Cruciani, M. Dondi, G. Gasparotto, and D.M. Tobaldi, J. Solid State Chem. **180**(11), 3196 (2007). https://doi.org/10.1016/j.jssc.2007.08.029
[41] P. Jeevanandam, Yu. Koltypin, and A. Gedanken, Mater. Sci. Eng. B, **90**(1-2), 125 (2002). https://doi.org/10.1016/S0921-5107(01)00928-X
[42] M. Jestl, I. Maran, A. Köck, W. Beinsting, and E. Gornik, Opt. Lett. **14**(14), 719 (1989). https://doi.org/10.1364/OL.14.000719
[43] A. Rahman, M.S. Charoo, and R. Jayaganthan, Materials Technology Adv. Perf. Mater. **30**(3), 1 (2015). https://doi.org/10.1179/1753555714Y.0000000211
[44] S.K. Sampath, D.G. Kanhere, and R. Pandey, J. Phys. Condens. Matter, **11**, 3635 (1999). https://doi.org/10.1088/0953-8984/11/18/301
[45] S. Suwanboon, T. Ratana, and T. Ratana, J. Sci. Technol. **4**(1), 111 (2007). https://wjst.wu.ac.th/index.php/wjst/article/view/129/111
[46] T. Takagahara, and K. Takeda, Phys. Rev. B, **46** 15578 (1992). https://doi.org/10.1103/PhysRevB.46.15578

ВПЛИВ ТЕМПЕРАТУРИ КАЛЬЦИНАЦІЇ НА СТРУКТУРНІ ТА ОПТИЧНІ ВЛАСТИВОСТІ НАНОЧАСТИНОК АЛЮМІНАТУ НІКЕЛЮ

Катрапалі Віджая Кумар[a], Сара Дурга Бхавані[b]
[a]Кафедра фізики, Інженерний коледж університету JNTUH Rajanna Sircilla, Аграхарам, район Раджанна Сірчілла, 505302, TS, Індія
[b]Кафедра хімії, Державний коледж, Раджендра Нагар, Хайдарабад, 500001, TS, Індія

Наночастинки алюмінату нікелю ($NiAl_2O_4$) синтезовано золь-гель методом з автоспалюванням. Підготовлені наночастинки були розділені на чотири частини та прожарені при 700, 900, 1100 і 1300°C і використані для цього дослідження. Захоплені наночастинки були охарактеризовані за допомогою порошкової рентгенівської дифракції (XRD), скануючої електронної мікроскопії (SEM), енергетичної дисперсійної рентгенівської спектроскопії (EDS), перетворення Фур'є та інфрачервоної (FT-IR) спектроскопії та спектроскопії UV-Vis. Рентгенівські дифрактограми підтвердили структуру шпінелі та просторову групу Fd3m. Формула Шеррера була використана для розрахунку розміру кристалітів і було знайдено розмір в діапазоні від 5,78 до 20,55 нм, тоді як параметр решітки був знайдений в діапазоні від 8,039 до 8,342 Å. Середній розмір зерна знаходився в діапазоні від 142,80 до 187,37 нм, тоді як міжплощинний відстань знаходився в діапазоні від 2,100 до 2,479 Å. Спектроскопія FTIR показала шість смуг поглинання в діапазоні від 400 до 3450 $см^{-1}$ і підтвердила структуру шпінелі. Ширина забороненої зони (Eg) зменшувалася з температурою прожарювання і знаходилася в діапазоні 4,2129 - 4,3115 еВ.

Ключові слова: *наночастинки алюмінату нікелю; метод золь-гель автозгоряння; температура прожарювання; розмір кристаліту; розмір зерен; елементний аналіз; ІЧ та УФ-видима спектроскопія*